UKAEA-CCFE-PR(19)28

Bogdan Hnat, Nick Walkden, The MAST Team

# Amplitude modulation and nonlinear self-interactions of the Geodesic Acoustic Mode at the edge of MAST

# Amplitude modulation and nonlinear self-interactions of the Geodesic Acoustic Mode at the edge of MAST

Bogdan Hnat, Nick Walkden, The MAST Team

This is a preprint of a paper submitted for publication in
Plasma-- Special Issue "Magnetic Confinement Fusion"

*Article*

# Amplitude modulation and nonlinear self-interactions of the Geodesic Acoustic Mode at the edge of MAST.

**Bogdan Hnat [1,†,‡], Nicholas Walkden[2,‡] and The MAST Team [2,*]**

[1] Physics Department, University of Warwick, Coventry CV4 7AL, UK; b.hnat@warwick.ac.uk
[2] EURATOM/CCFE Fusion Association, Culham Science Centre, Abingdon, OX14 3DB, United Kingdom
* Correspondence: e-mail@e-mail.com; Tel.: (optional; include country code; if there are multiple corresponding authors, add author initials) +xx-xxxx-xxx-xxxx (F.L.)
† Current address: Affiliation 3
‡ These authors contributed equally to this work.

Version March 21, 2019 submitted to Journal Not Specified

**Abstract:** We study the amplitude modulation of the radial electric field constructed from the Langmuir probe plasma potential measurements at the edge of MAST. The Empirical Mode Decomposition technique is applied, which allows us to construct fluctuations on temporal scales of plasma turbulence, the Geodesic Acoustic Mode and these associated with the residual poloidal flows. This decomposition preserves nonlinear character of the signal. Hilbert transform is then used to obtain the amplitude modulation envelope of the fluctuating radial electric field on these time scales. We find significant spectral coherence at frequencies between $1-5$ kHz, in the turbulence and the GAM amplitude modulation envelopes and for the signal representing the low frequency zonal flows. We find evidence of local and nonlocal three wave interactions leading to coupling between the GAM and the low frequency part of the spectrum.

**Keywords:** Fusion plasma; radial electric field; temporal intermittency)

## 1. Introduction

The edge region of tokamaks, defined by the steep pressure gradient, is dominated by turbulent structures of density, temperature and the electrostatic potential (see, for example, [1] and the references therein) arising from resistive and/or interchange plasma instabilities. These fluctuations are responsible for the intermittent turbulent radial transport, which drives core heat and particle losses. Thus, better understanding and control of the edge transport is fundamental to enabling enhanced plasma confinement scenarios of future fusion reactors. The anisotropic shear amplification of micro-turbulence Reynolds stress produces radially localised, toroidally and poloidaly symmetric flows, called zonal flows (ZF). These flows are distinct from the residual poloidal flows, often called zero frequency zonal flows (ZFZF) [2,3]. Shearing associated with both types of zonal flows can nonlinearly modify stability threshold of unstable plasma modes [4–6] and reduces turbulence level by vortex stretching [7,9].

Zonal flows are axisymmetric electrostatic potential modes with zero poloidal and toroidal numbers, $m=n=0$. In tokamak geometry, toroidal curvature couples ZF to the density perturbations with poloidal mode numbers $m \geq 1$ ($n=0$), and with a finite frequency. This compressible component of ZF is called Geodesic Acoustic Mode (GAM). The local dispersion relation for the GAM has been derived from various plasma models and the leading term is $\omega_{G,l} \sim c_s/R_0$, where $c_s$ is the local sound speed and $R_0$ is the major radius [10,11]. The amplitude of the density fluctuations varies with the poloidal angle $\theta$ as $A \sim \sin(\theta)$. Since its theoretical discovery, the GAM has been experimentally observed in many tokamaks [12–16]. While the local theory predicts a monotonic change of the observed GAM frequency with a radius, due to temperature gradient, there is growing evidence that the GAM is a global mode with a complex radial mode structure [17–20]. Driven by turbulent fluctuations [21], ZF and GAM provide a natural sink for turbulent energy. The stability of these flows is less understood. The GAM is damped by a Landau mechanism, in the region of low safety factor $q(r)$. The ZF/GAM can decay via nonlinear tertiary K-H instability of small scale fluctuations [5,21]. Nonlinear advection of GAM pressure perturbations provides a mechanism for the energy transport from ZF back to micro-turbulence scales [22,23].

Nonlinear interaction of ZF/GAM with turbulence are fundamental to our understanding of the L-H transition [8,24]. In this context, GAM is a valuable tool in the experimental studies of ZF due to its finite frequency, which allows easier identification of ZF in experimental data [19]. Here, we study the coupling of GAM/ZF and turbulence by examining the low frequency amplitude modulations of the oscillating radial electric field component on different temporal scales. It has been observed before that the power associated with the radial electric field oscillations at GAM frequency is not uniform in time. Instead, it shows strong temporal intermittency, that is, the power is concentrated in few intense temporal regions, separated by intervals of low level activity. We use Hilbert transform based techniques to extract radial electric field fluctuations on different temporal scales while preserving their nonlinear character. This allows us to construct signals representing meso-scale turbulence, the oscillatory GAM signal and the low frequency zonal flows, ZFZF. Hilbert transform gives nonlinear envelopes for the turbulence and the GAM. The spectralcoherence of the turbulence with the GAM is then examined. We find that the amplitude modulation of the turbulence and the GAM have a similar behaviour at low frequencies, between $2-5$ kHz. The auto bi-coherence reveals nonlinear self-interaction of GAM and the possible coupling to these low frequency components.

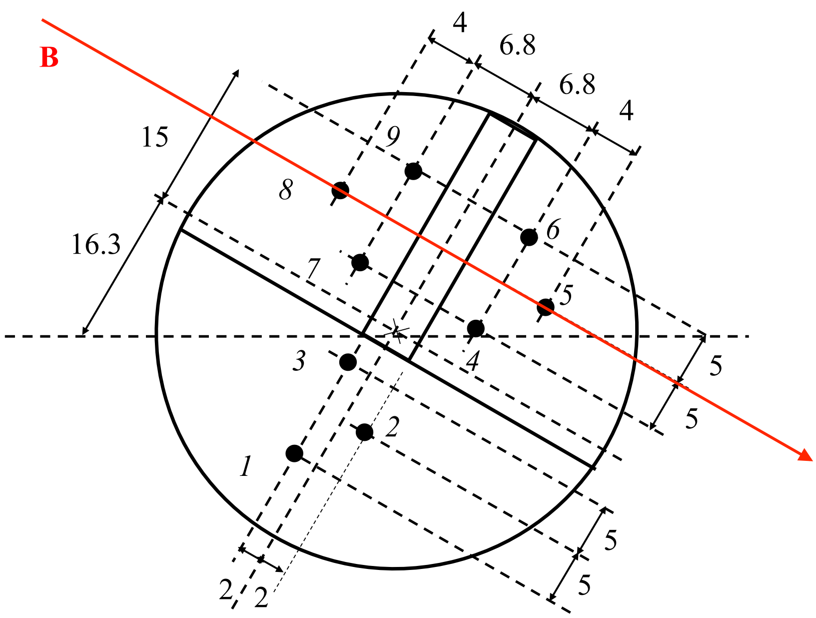


**Figure 1.** (a) Langmuir Mach probe with separations of different pins in millimetres. Pins 1,2 and 3 are radially offset by 8mm from all other pins.

## 2. Experimental setup and data

The Mega Amp Spherical Tokamak (MAST) has a major radius $R_0 \approx 0.85$ m and a minor radius of $a \approx 0.65$ m. The magnetic field strength is about 0.5T with the toroidal, $B_\zeta$, and the poloidal, $B_\theta$, field components giving a pitch angle of about 22° at the edge of the device. We analyse data from an Ohmic plasma discharge numbered 29150, with a line average number density, $n \approx 1.47 \times 10^{19}$ m$^{-3}$, and plasma current $I_p = 0.43$MA. No additional heating power was applied during the discharge. Magnetic configuration was a double null.

The data was collected using a Mach type reciprocating Langmuir probe [25], on the outboard mid-plane, measuring floating potential, $\tilde{V}_f$ as well a set of ion saturation currents (pins 2, 5 and 8). Figure 1 shows the schematic of the probe, with pin numbers and the relative distances between them. Pins $(1,3)$ are positioned 0.8 cm behind pin pairs $(4,6)$ and $(7,9)$. We assume that the floating potential $\tilde{V}_f$ is a good proxy of the plasma potential $\tilde{V}_p$. These are related by $\tilde{V}_p = \tilde{V}_f + \Lambda$, where $\Lambda$ is the sheath potential drop, which is a slowly varying function of the electron and ion temperatures and is usually approximated by $\Lambda \approx 2.5T_e/e$ [26]. It is assumed that the electrostatic potential fluctuations are larger then these due to electron/ion temperature fluctuations. The sheath potential of the Mach barrier can modify plasma flows as well as the electron and the ion temperatures, but the measurement of $\tilde{V}_f$ is based on the ion and electron currents balance, which in principle should depend only on the plasma temperature. The high values of temporal correlations on all pin pairs, with correlation coefficients between 0.65 and 0.95 are consistent with these assumptions. We construct radial electric field component $E_r$ by differencing the floating potential values on pin pair (1,9), $E_r = \nabla_r \tilde{V}_p \approx (\tilde{V}_p^1 - \tilde{V}_p^9)/d_r^{(1,9)}$, where the superscripts on the floating potential indicates a pin and $d_r^{(1,9)} = 0.8$ cm is a radial separation of these pins. We note that the poloidal separation of the pin pair $(1,9)$, $d_\theta^{(1,9)} = 3.8$ cm, is much larger than the radial separation. This minimises the impact of large poloidal wave numbers, associated with turbulence, on the radial electric field estimation. We have chosen time interval of $0.315 - 0.33$, during which the intermittent character of the fluctuations is clearly present.

Figure 2 presents a summary of the data. Panel (a) shows the time series of the radial electric field $E_r(t)$, containing approximately 7500 samples. Assuming that the toroidal magnetic field is dominant, the radial electric field gives the poloidal flow speed $v_\theta = (E_r B_\phi)/B^2$. Panel (b) shows the distance of the Mach probe in relation to the last closed flux surface (LCFS) during this time interval. The probe is inside the plasma its radial depth varies between $\sim$4 and $\sim$5 cm. Panel (c) of Figure 2 shows electron temperature from Thomson scattering diagnostic at the time of interest. It gives the median of electron temperature at the probe location of $T_e \approx 14$ eV. We take the electron temperature at $T_e = 10$ eV in all calculations that follow. The proton gyroradius at this electron temperature is $\rho_p = 0.15$ cm.

## 3. Methods

The methods based on the Hilbert-Huang transform (HHT) offer a natural approach to studying temporal intermittency in a time series. The intermittency is interpreted as an amplitude modulation of a mode, or a group of modes, of interest. Here, we employ this method as an effective filter, which allows us to construct signals representing different dynamical temporal scales. The HHT performs well when analysing non-stationary and non-harmonic fluctuations arising in nonlinear systems. Fourier-based spectral techniques as well as the wavelet transform are unsuitable for such time series if the principal aim is to preserve the nonlinear nature of the wave trains. The HHT makes use of the Empirical Mode Decomposition (EMD) [27], which expands the input signal onto a set of intrinsic mode functions (IMFs) derived directly from the data.

In practice, the iterative sifting process is performed as follows: firstly, the maxima and minima of the signal are separately connected using cubic splines to form two envelopes of the data; one that contains all of the maxima and the other, the minima. The mean of the maximum and minimum envelopes, $m_1$, is calculated. For an input signal $S(t)$, the difference, $h_1 = S(t) - m_1$ gives the first estimation of the envelope of $S(t)$. However, this envelope's mean is, in general, not equal to the true local mean, especially if the data is nonlinear. The process is therefore repeated $k$ times until the resultant, $h_{1k}$, satisfies the requirement for an IMF, $h_{1(k-1)} - m_{1k} = h_{1k}$, where $h_{ik}$ and $m_{ik}$ are the $i$th

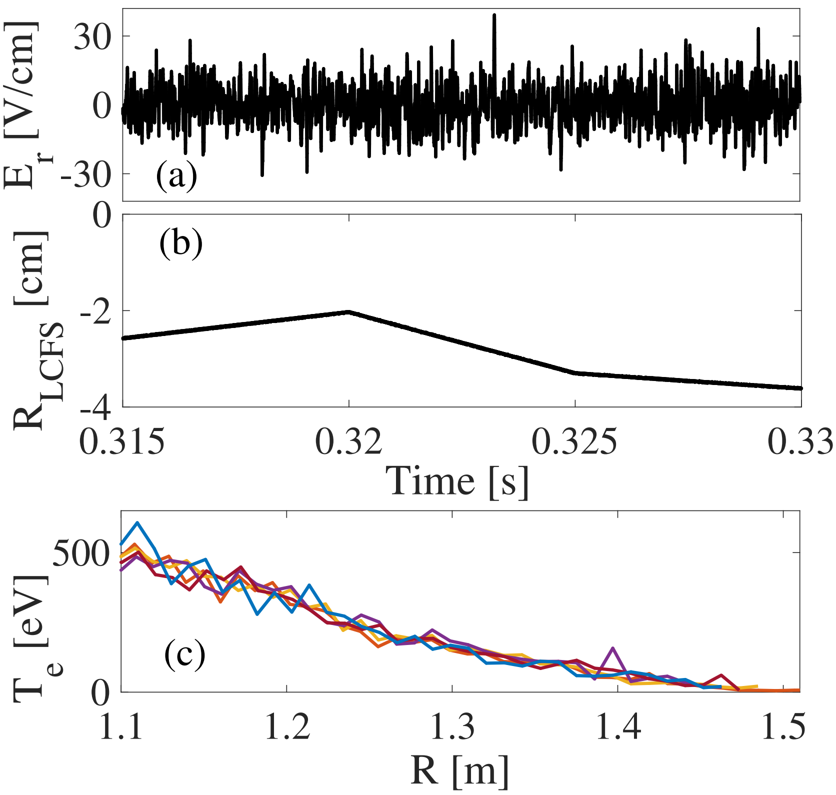


**Figure 2.** Summary of the data. (a) Wavelet power at lower frequencies. (b) Mach probe distance from the last closed flux surface (LCFS); negative values indicate position inside the plasma. Horizontal red lines mark three time intervals analysed here. (c) Electron temperature profiles from Thompson scattering system between $0.32 - 0.36$ seconds.

envelope and its mean after $k$th sifting iteration, accordingly. We then designate $s_1(t) = h_{1k}$ as the first IMF component of the data, containing the shortest period of the signal. Fluctuations at this scale are removed from the data to obtain a residual $r_1 = S(t) - s_1(t)$. The procedure is then repeated for the residual $r_1$, treated as a new input signal. The decomposition is stopped either when the component $s_i$, or the residue $r_i$, become too small to be of interest, or when the residue, $r_i$, becomes a monotonic function from which no more IMFs can be extracted. For data with a trend, the final residue should be that trend. When the process is finished, we obtain the decomposition of a signal $S(t)$ into IMFs $s_i$ and the final residue:

$$S(t) = \sum_{i=1}^{N} s_i(t) + r_N. \tag{1}$$

The IMFs may contain oscillations with different periods in one mode, and different modes can contain similar periods. This spectral leakage, or mode mixing, can be an issue, especially for short and intermittent data. We incorporate the ensemble empirical mode decomposition (EEMD) [28,29] to reduce the impact of mode mixing. This noise-assisted method adds white noise to the original data before the sifting process starts. The EMD modes are computed as normal until all of the IMFs are calculated. The original data is then reprocessed with a different noise realisation and the final IMF is averaged over all ensembles. In this work we use EEMD to decompose the radial electric field time series into a number of IMFs. We are interested in the amplitude modulation of turbulence and the

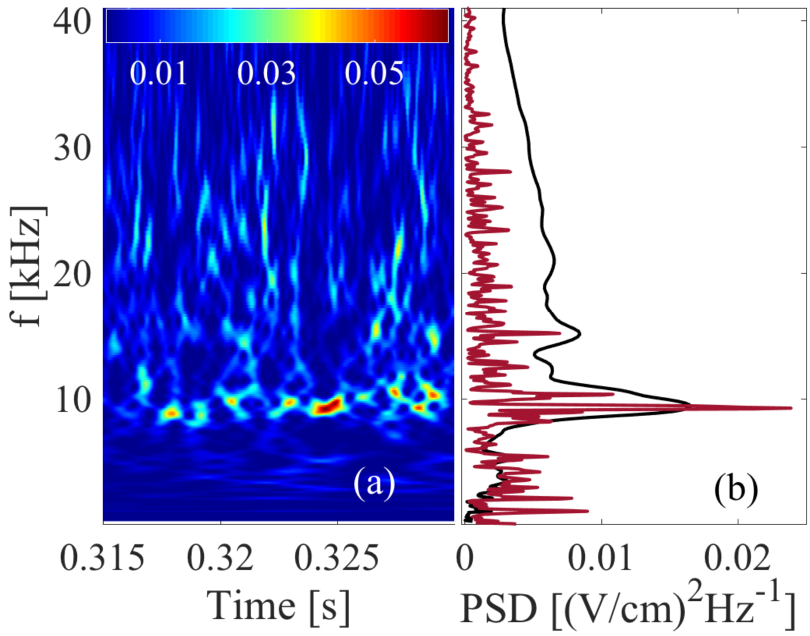


**Figure 3.** (a) Wavelet dynamic spectrum of $E_r(t)$. (b) Integrated wavelet power spectrum (black) and Fourier spectrum estimate (red). A significant spectral peak at $\sim$10 kHz is clearly seen. Fourier spectrum shows an internal structure of the GAM peak, with multiple modes separated by $\sim$1 kHz. A possible second harmonic is also present at $\sim$20 kHz.

Geodesic Acoustic Mode (GAM). The modes with the periods shorter than the GAM are interpreted as turbulence. An envelope of a modulated signal can be constructed using analytic signal $S_a$:

$$S_a(t) = S(t) + i\mathcal{H}[S(t)] = E(t)\exp[i\phi(t)], \tag{2}$$

where $\mathcal{H}[S(t)]$ indicates Hilbert transform of the signal $S$, and $i^2 = -1$. For a slowly modulated signal the modulus of $S_a$ corresponds to the amplitude modulation envelope $E(t)$. The frequency of $S_a$, which may not be be constant in time, can be obtained from the mean of the instantaneous phase change $f = \langle d\phi/dt \rangle$.

In order to quantify the nonlinear interactions between different modes we use the wavelet bi-coherence defined as

$$b^2(f_1, f_2) = \frac{|\langle \tilde{S}(f_1,\tau)\tilde{S}(f_2,\tau)\tilde{S}^*(f_1+f_2,\tau)\rangle|^2}{\langle|\tilde{S}(f_1,\tau)\tilde{S}^*(f_2,\tau)|^2\rangle\langle|\tilde{S}(f_1+f_2,\tau)|^2\rangle}, \tag{3}$$

where $\tilde{S}$ is a wavelet coefficient at a scale associated with a period $1/f$ and at time $\tau$. For a signal $S(t)$, the wavelet coefficients are given by

$$\tilde{S}(s,\tau) = \int_{-\infty}^{\infty} dt S(t)\frac{1}{\sqrt{s}}\psi^*\left(\frac{t-\tau}{s}\right), \tag{4}$$

where $s$ is a temporal scale, $\tau$ is a new time label and $\psi(t)$ is the analysing wavelet. We use Bump wavelets [30], which have better frequency resolution, but poorer time localisation compared with a standard Morlet wavelet. Given a set of wavelet coefficients $\tilde{S}(f,\tau)$ the wavelet spectrum estimate is given by

$$P(f) = \langle \tilde{S}^*(\nu,\tau)\tilde{S}(\nu,\tau)\rangle_\tau. \tag{5}$$

Wavelet estimates of the bi-coherence are superior to these obtained form the Fourier transform for shorter and non-stationary data sets. Fourier-based bi-coherence requires the averaging over many realisations of the same data, while the averaging indicating by $\langle \ldots \rangle$ in (3) is over time.

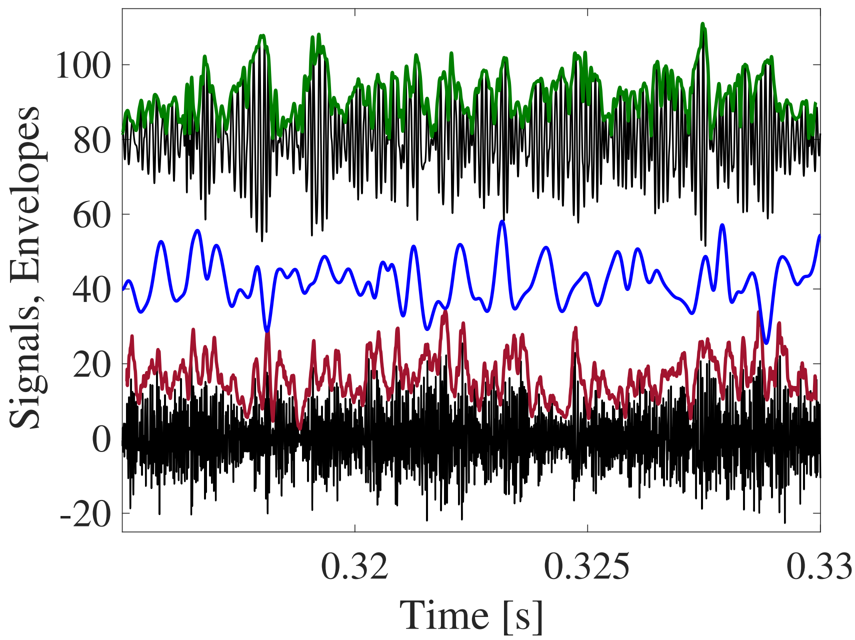


**Figure 4.** Signals constructed from EMMD produced IMFs: turbulence $S_T$ (lower, black), the GAM $S_G$ (upper black) low frequency zonal flows $S_Z$ (blue). Envelopes of turbulence $E_T$ (red) and of the GAM (green) obtained from the analytic signal method. Both, the GAM and ZFZF were offset vertically for clarity.

## 4. Results

A strong oscillatory component has been previously identified in MAST edge plasma density and electrostatic potential fluctuations measured by the reciprocating Langmuir probes [15,20]. This mode shows a spectral power peak at the frequency of $\sim$10 kHz, in a reasonably good agreement with the theoretical and numerical predictions for GAM frequency in MAST L-mode edge plasma [15,16]. Panel (a) of figure 3 shows the wavelet transform dynamic spectrum for the radial electric field. The intermittent series of power maxima are clearly visible around the predicted GAM frequency of $\sim$10 kHz. The integrated wavelet spectrum of electric field fluctuations is shown in the panel (b) of the same figure. The spectral peak at $\sim$10 kHz is approximately 4 times above the power level of turbulent fluctuations at neighbouring frequencies. We note an apparent second harmonic peak at $\sim$20 kHz and a complex number of smaller maxima at frequencies below $\sim$5 kHz. We also show the Fourier power spectrum estimation for the same signal in the red trace, which reveals multiple peaks within a single broad spectral peak of a wavelet spectrum estimate. These additional spectral peaks in the Fourier-based spectrum are separated from the main peak by no more than 1 kHz. Allowing non-linear interactions between the modes represented by the peaks clustering around $\sim$10 kHz, could lead to low-frequency modulation in the electric field signal.

In order to study the GAM amplitude modulation and its possible impact on turbulence and ZFs, we decompose our data into three components with distinct temporal scales: turbulence, GAM and low frequency zonal flow (ZFZF). We use the EEMD technique to generate 25 IMFs from the original, $E_r$ data, with the largest frequency of about $\sim$115 kHz and the smallest frequency at $\sim$70 Hz. The largest frequency is treated as the residual noise in the data and is discarded. Similarly, we discard he smallest frequency mode, which is a nonlinear trend very close to zero. We then combine the IMFs at three different frequency ranges to obtain signals of interest. The turbulence, $S_T(t)$, is a superposition of IMF $2-4$, corresponding to mean instantaneous frequencies between $\sim$25 kHz and $\sim$66 kHz. The GAM is a single IMF with the mean frequency of 10 kHz, $S_G(t)$. Finally, the ZFZFs signal $S_Z(t)$ is obtained by summing modes $8-20$, with mean frequencies in the range $77-5000$ Hz. We apply an analytic signal approach to $S_T$ and $S_G$, in order to obtain their amplitude modulation envelopes $E_T$ and $E_G$, respectively. The turbulence envelope is smoothed over 50 neighbouring points. Figure 4 shows signals and their upper envelopes. The GAM, its envelope and the ZFZF signal have been shifted vertically and their amplitudes were modified for clarity. A close visual inspection is sufficient to see that there is no phase coherence between turbulence envelope, GAM envelope and the ZFZF signal. This is confirmed by a linear cross correlation coefficients calculated for the pairs $(E_T, E_G)$, $(E_T, S_Z)$ and $(E_G, S_Z)$, which had values at around or below 0.25, at different non-zero time lags.

While there is no phase coherence in the low-frequency behaviour of $E_T$, $E_G$ and $S_Z$, there is a considerable spectral coherence for these time traces. Figure 5 shows Fourier spectral estimate of power for $E_T$, $E_G$ and $S_Z$ in panels (a), (b) and (c) respectively. Note that all spectra have been normalised to their respective maxima, which had a value of 0.05 for turbulence envelope, 0.28 for the GAM envelop and 0.008 for ZFZF signal. All spectra have pronounced peaks at about 1 kHz and at 2 kHz. The GAM envelope spectrum shows a number of peaks at relatively constant increments, positioned at $\sim$0.55, $\sim$0.75, 1 and 1.5 kHz. We also note that, the ZFZF spectrum shows a broad spectral power between frequencies $3-5$ kHz. This is a strong suggestion that there are nonlinear interactions between various modes, close to the GAM frequency, and also non-local between GAM/turbulence and ZFZF.

The resonant tree wave interaction process is considered as a model of coupling between different modes present in the radial electric field time series. For a single point time series measurements, we can only consider frequency resonances $f_3 = f_1 + f_2$. The strength of these interactions is then approximated by a bi-coherence, which we have calculated using wavelet coefficients and averaged over all times. Figure 6 shows only positive frequency part of the bi-coherence, which was thresholded at a relatively high value of 0.7 to emphasise the most relevant interactions. We find the signature of strong local interactions at the GAM frequencies $f_1 \approx f_2 \approx 10$ kHz, positioned on the diagonal line, as well as non-local interactions with the low frequency modes such as $f_1 = 8.4$ kHz, $f_2 = 1.2$ kHz. Interestingly, the bi-coherence also reveals the importance of a mode with $f \approx 4$ kHz, which also self-interacts and couples to low frequency modes.

## 5. Discussion

We have performed the analysis of the fluctuations in the radial electric field component obtained from the reciprocating Langmuir Mach probe at the mid plane of MAST. Wavelet dynamic spectrum reveals temporal power intermittency of the GAM, while Fourier spectrum estimate revealed multiple spectral peaks in the vicinity of 10 kHz. We use Hilbert-Huang transform based technique, EEMD, to extract radial electric field fluctuations on temporal scales of turbulence, the GAM and ZFZF. Envelopes of turbulent signal and the GAM were constructed using analytic signal approach. We found a significant spectral coherence for the turbulent envelope, GAM envelope and the low frequency component. The bi-coherence revealed strong nonlinear interactions, local self-interactions near the GAM frequency [31], and non-local interactions with low frequency mediated by the GAM. This is broadly consistent with previous results presented in the literature [19,32].

Our findings may be of particular importance for better understanding how the presence of the GAM alters the physics of L-H transition. It has been reported that the low frequency component, which we have termed ZFZF in this work, increases significantly at the expense of the GAM during the transition [24]. The energy flow for the three component system, turbulence, GAM and ZF, is often modelled using nonlinear predator-prey type formulation [2,33]. These models incorporate all key physical interactions important for the dynamics of the system, but retain simplicity that allows better understanding of how each component effects their collective complex dynamics, for example, the L-H

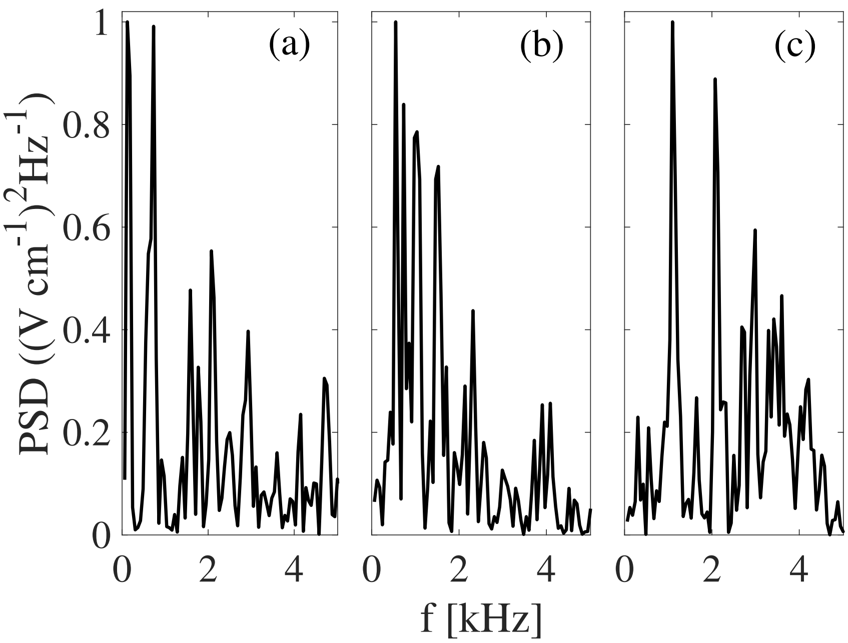


**Figure 5.** Fourier spectra of: (a) turbulence envelope $E_T$, (b) GAM envelope $E_G$ and (c) of ZFZF signal $S_Z$.

transition. The behaviour of these models is strongly influenced by the included interactions between various components. This work clearly shows that in addition to the linear impact of the GAM on ZFs [34], the nonlinear interactions are also important.

**Author Contributions:** Conceptualization, B.H. ; methodology, B.H.; data curation, N.W. and MAST Team

**Acknowledgments:** This work has been carried out within the framework of the EUROfusion Consortium and has received funding from the Euratom research and training programme 2014-2018 under grant agreement No 633053 and from the RCUK Energy Programme [grant number EP/P012450/1]. The views and opinions expressed herein do not necessarily reflect those of the European Commission.

## References

1. Zweben SJ, Boedo JA, Grulke O, Hidalgo C, LaBombard B, Maqueda RJ, Scarin P, Terry JL. Edge turbulence measurements in toroidal fusion devices. *Plasma Physics and Controlled Fusion* **2007**, *49*, S1.
2. Diamond, P.H., Itoh, S.I., Itoh, K. and Hahm, T.S. Zonal flows in plasma-a review. *Plasma Phys. Controlled Fusion* **2005**, *47*, R35–R161.
3. Rosenbluth, M.N. and Hinton, F.L. Poloidal flow driven by ion-temperature-gradient turbulence in tokamaks. *Physical Review Letters* **1998**, *80*, 724–727.
4. Dimits A.M., Bateman G., Beer M.A., Cohen B.I., Dorland W., Hammett G.W., Kim C., Kinsey J.E., Kotschenreuther M., Kritz A.H., Lao L.L. Comparisons and physics basis of tokamak transport models and turbulence simulations. *Physics of Plasmas* **2000** *7*, 969–83.
5. Numata R., Ball R., Dewar R.L. Bifurcation in electrostatic resistive drift wave turbulence. *Physics of Plasmas* **2007** *26*, 102312.
6. Gadgil S, Hnat B, Rowlands G. Investigation of drift-wave instability in the presence of zonal flows using spatial averaging. *Physics of Plasmas* **2019** *26*, 012105.
7. Lin, Z., Hahm, T.S., Lee, W.W., Tang, W.M. and White, R.B., 1998. Turbulent transport reduction by zonal flows: Massively parallel simulations. *Science* **1998**, *281*, 1835–1837.
8. Moyer, R.A., Tynan, G.R., Holland, C. and Burin, M.J. Increased Nonlinear Coupling between Turbulence and Low-Frequency Fluctuations at the L-H Transition. *Physical Review Letters* **2001**, *87*, 135001.

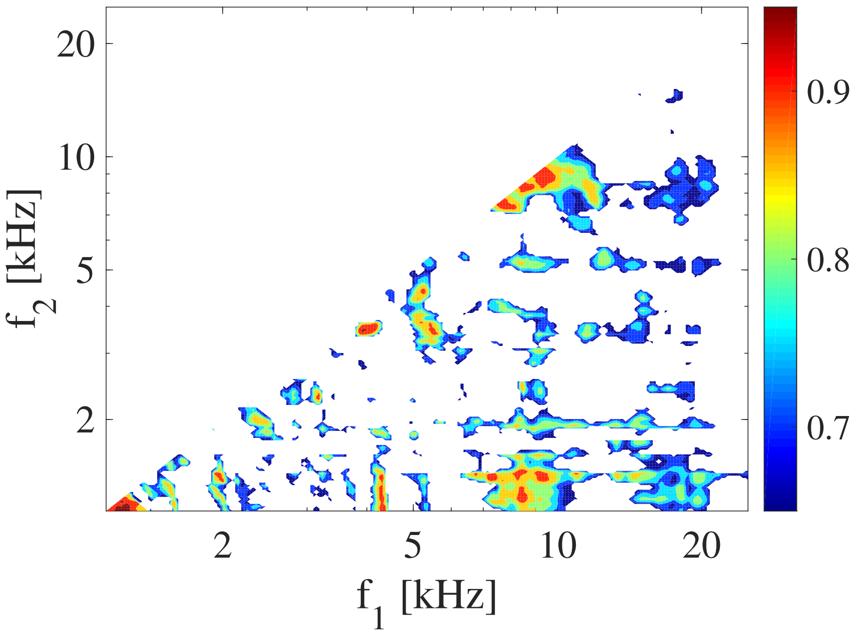


**Figure 6.** The wavelet bi-coherence for the entire data set $E_r$.

9. Tynan, G.R., Moyer, R.A., Burin, M.J. and Holland, C., 2001. On the nonlinear turbulent dynamics of shear-flow decorrelation and zonal flow generation. *Physics of Plasmas* **2001**, *8*, 2691–2699.
10. Winsor, N., Johnson, J.L. and Dawson, J.M. Geodesic acoustic waves in hydromagnetic systems. The Physics of Fluids **1968**, *11*, 2448–2450.
11. Gao Z. Collisional damping of the geodesic acoustic mode. *Physics of Plasmas* **2013** *20*, 032501.
12. Jakubowski, M., Fonck, R.J. and McKee, G.R., Observation of coherent sheared turbulence flows in the DIII-D tokamak. *Physical Review Letters* **2002**, *89*, 265003.
13. Silva, C., Arnoux, G., Groth, M., Hidalgo, C., Marsen, S. and JET-EFDA Contributors, Observation of geodesic acoustic modes in the JET edge plasma. *Plasma Physics and Controlled Fusion* **2012**, *55*, 025001.
14. Ido T, Miura Y, Kamiya K, Hamada Y, Hoshino K, Fujisawa A, Itoh K, Itoh SI, Nishizawa A, Ogawa H, Kusama Y. Geodesic acoustic mode in JFT 2M tokamak plasmas. *Plasma Physics and Controlled Fusion* **2006**, *48*, S41–S50.
15. Robinson, J.R., Hnat, B., Dura, P., Kirk, A., Tamain, P. and MAST Team, 2012. Interaction between a low-frequency electrostatic mode and resonant magnetic perturbations in MAST. *Plasma Physics and Controlled Fusion* **2012**, *54*, 105007.
16. Robinson, J.R., Hnat, B., Thyagaraja, A., McClements, K.G., Knight, P.J., Kirk, A. and MAST Team, Global two-fluid simulations of geodesic acoustic modes in strongly shaped tight aspect ratio tokamak plasmas. *Physics of Plasmas* **2013**, *20*, 052302.
17. Itoh, K., Itoh, S.I., Diamond, P.H., Fujisawa, A., Yagi, M., Watari, T., Nagashima, Y. and Fukuyama, A., Geodesic acoustic eigenmodes. *Plasma and Fusion Research* **2006**, *1*, 037-037.
18. Miyato, N., Kishimoto, Y. and Li, J.Q., 2006. Nonlocal behaviour of zonal flows in tokamak plasmas. *Plasma Physics and Controlled Fusion* **2006**, *48*, A335.
19. Liu, A.D., Lan, T., Yu, C.X., Zhao, H.L., Yan, L.W., Hong, W.Y., Dong, J.Q., Zhao, K.J., Qian, J., Cheng, J. and Duan, X.R., Characterizations of low-frequency zonal flow in the edge plasma of the HL-2A tokamak. *Physical Review Letters* **2009**, *103*, 095002.
20. Hnat B, Gadgil S, Kirk A, Militello F, Walkden N, MAST Team. Experimental constraint on the radial mode number of the geodesic acoustic mode from multi-point Langmuir probe measurements in MAST Ohmic plasma. *Plasma Physics and Controlled Fusion* **2018** *60*, 085016.

21. Rogers, B.N., Dorland, W. and Kotschenreuther, M. Generation and stability of zonal flows in ion-temperature-gradient mode turbulence. *Physical Review Letters* **2000**, *85*, 5336–5339.
22. Scott, B., The geodesic transfer effect on zonal flows in tokamak edge turbulence. *Physics Letters A* **2003**, *320*, 53–62.
23. Fujisawa A, Shimizu A, Nakano H, Ohshima S, Itoh K, Nagashima Y, Itoh SI, Iguchi H, Yoshimura Y, Minami T, Nagaoka K. Intermittent characteristics in coupling between turbulence and zonal flows. *Plasma Physics and Controlled Fusion*. **2007**, *49*, 211–217.
24. Team AU, Conway GD, Angioni C, Ryter F, Sauter P, Vicente J. Mean and oscillating plasma flows and turbulence interactions across the L-H confinement transition. *Physical Review Letters* **2011**, *106*, 065001.
25. MacLatchy, C.S., Boucher, C., Poirier, D.A. and Gunn, J., Gundestrup: A Langmuir/Mach probe array for measuring flows in the scrape-off layer of TdeV. *Review of scientific instruments* **1992**, *63*, 3923–3929.
26. Tamain, P., Kirk, A., Nardon, E., Dudson, B. and Hnat, B., Edge turbulence and flows in the presence of resonant magnetic perturbations on MAST. *Plasma Physics and Controlled Fusion* **2010**, *52*, 075017.
27. Huang NE, Shen Z, Long SR, Wu MC, Shih HH, Zheng Q, Yen NC, Tung CC, Liu HH. The empirical mode decomposition and the Hilbert spectrum for nonlinear and non-stationary time series analysis. *Proceedings of the Royal Society of London. Series A: Mathematical, Physical and Engineering Sciences* **1998**, *454A*, 903–995.
28. Wu Z, Huang NE. Ensemble empirical mode decomposition: a noise-assisted data analysis method. *Advances in adaptive data analysis* **2009**, *1*, 1–41.
29. Torres ME, Colominas MA, Schlotthauer G, Flandrin P. A complete ensemble empirical mode decomposition with adaptive noise, in: *Proc. 36th IEEE Int. Conf. on Acoust., Speech and Signal Process, ICASSP* **2011**, Prague, Czech Republic, 4144–4147.
30. https://uk.mathworks.com/help/wavelet/ref/cwtftinfo.html
31. Sasaki, M., Itoh, K., Nagashima, Y., Ejiri, A. and Takase, Y., Nonlinear self-interaction of geodesic acoustic modes in toroidal plasmas. *Physics of Plasmas* **2009**, *16*, 022306.
32. Ramisch M, Stroth U, Niedner S, Scott B. On the detection of Reynolds stress as a driving and damping mechanism of geodesic acoustic modes and zonal flows. *New Journal of Physics* **2003**, *4*, 1–12;
33. Miki, K. and Diamond, P.H., 2010. Role of the geodesic acoustic mode shearing feedback loop in transport bifurcations and turbulence spreading. *Physics of Plasmas*, 17(3), p.032309.
34. Hallatschek K, Biskamp D. Transport control by coherent zonal flows in the core/edge transitional regime. *Physical Review Letters* **2001**, *12*, 1223–1227.